Benha Journal of Applied Sciences (BJAS) **print: ISSN 2356–9751**
Vol. (10) Issue (7) (2025), (55- 72) **online: ISSN 2356–976x**
https://bjas.journals.ekb.eg/
engineering sciences

Novel simulation method for TFET-based ISFET pH sensor

Eman A.Hassan, Mina D.Asham, Walid Soliman and Tarek M.Abdolkader
Basic Engineering Science Dept., Benha Faculty of Engineering, Benha, Egypt.
E-mail: eman.adel@bhit.bu.edu.eg

Abstract

Ion-Sensitive Field-Effect Transistors (ISFETs), which were initially proposed a little more than 50 years ago, are currently among the most widely used electrochemical biosensors. In this work we propose a numerical simulation methodology for nanoscale ISFETs that is based on band-to-band tunneling conduction mechanism. The proposed method is based on the combination of the analytical equations of Tunneling Field-Effect Transistors (TFETs) with the Gouy–Chapman–Stern model equations of ISFETs. We then get a system of equations of Ion-Sensitive Tunneling Field-Effect Transistors (ISTFETs) that can be solved iteratively to produce output current and sensor sensitivity. The simulation is implemented using MATLAB software tool. The simulation results are verified by comparing the results of the developed code with Silvaco TCAD simulation software. The simulation code is then used for the optimization of the sensitivity and linearity of nanoscale ISFETs. We investigate the effect of various parameters, such as drain current level, reference voltage, gate-insulator thickness, substrate thickness, and temperature, on the sensor performance. Additionally, the effect of using different gate-insulator materials is inspected by comparing three different insulator types: SiO_2, Al_2O_3, and HfO_2. The simulation method can be applied to both single-gate and double-gate devices and serves as a guide for the design and optimization of nanoscale ISFETs.

Keywords: pH sensor, ISTFET, TFET, Sensitivity, numerical modelling

1. Introduction

The Ion Sensitive Field Effect Transistor (ISFET) is one of the promising miniature chemical sensors that has drawn a lot of attention from researchers as a possible electrical biosensor. This is due to its many advantages like reusability, portability, low power consumption, low cost, quick detection, and compatibility with existing CMOS technology [1 - 3].

ISFET is a form of potentiometric biosensor that functions similarly to a traditional MOSFET (Metal Oxide Semiconductor Field-Effect Transistor). The process for fabricating ISFETs is straightforward and comparable to that of producing MOSFETs. Yates et al. proposed the site-bending concept in 1974 [4], which explains the ISFET theory of operation. It explains the formation of ion pairs at the well-known electrolyte interface method for defining ion-sensing applications in oxide/aqueous ISFETs.

ISFET is effective in detecting ions and biomolecules such as cell-related chemicals,antibodies, enzyme, and DNA molecules. Basically, ISFET senses the concentration of ions in a solution by measuring how this concentration modulates the electrostatic potential at the gate-insulator interface, which translates to a comparable change in the drain current of the device.

Conventional Field-Effect-Transistors (FETs) such as MOSFETs suffer from many problems, such as long response time, high off-state current, degradation of subthreshold slope (SS) (SS > 60 mV/decade). The sensitivity of ISFET-based on MOSFET devices can't exceed the Nernst limit [4, 5]. According to the Nernst limit, ISFET devices can achieve a maximum sensitivity of 59 mV/pH at room temperature [7]. Higher sensitivity means that acceptable detection capability of a lower concentration of analyte or smaller molecules of samples is achieved by the device. In order to achieve sensitivity over the Nernst limit, research on ISFET has been conducted using a variety of techniques, including experimental characterization [7 - 9], modeling, and simulation [10 ,11].

One of the newest nano-electronic devices is the Tunnel-Field Effect Transistor (TFET). Due to its low subthreshold swing (SS) ((SS) < 60 mV/dec), low off-state current, and low power consumption compared with traditional MOSFETs, TFET is becoming more and more popular in comparison to MOSFET[13]. In addition, TFET is also impervious to short-channel effects [14]. An Ion-Sensitive Tunneling Field-Effect Transistor (ISTFET) exhibits higher sensitivity than its conventional MOSFET-based equivalents and in addition, it has a relatively shorter response time because of the band-to-band tunneling phenomenon. As a result, TFET-based biosensors are receiving increased interest for sensing applications[15]. Nevertheless, there has not been a thorough examination of the TFET underlap architecture with the electrolyte/watery solution until now [7].

In this study, we present a numerical simulation approach for nanoscale ISFETs that combines the Gouy–Chapman–Stern model equations of ISFET [16] with the nanoscale TFET equations put forth by T.S. Arun Samuel [17] to create a system of equations that

can be solved iteratively to produce ISFET output current. MATLAB software is used to write the tool's code. Both single-gate and double-gate ISFETs can be simulated using the developed tool.

We provide a brief overview of single-gate TFET modeling [17] in Section 2 and theory of ISFET modeling in Section 3. In Section 4, we demonstrate the specifics of the proposed simulation method, and the results and their discussion are presented in Section 5, which is followed by the conclusion.

2. Modeling of TFET:

This section presents the TFET modeling [17].As will be discussed in Section 4, this modeling will be used to simulate ISTFET by merging TFET model equations with Gouy–Chapman–Stern model equations of conventional ISFET. We assume here an n-type TFET such that the drain region is made of n-type material, the source region is made of *p*-type material, and the channel region is made of intrinsic material. **Figure. 1** shows the energy band diagram of TFET at both OFF and ON state with black and red lines, respectively. In the OFF state, electrons in the conduction band of the *p*+-type source are so few that only a negligible current can flow from the source to the drain. On the other hand, in the ON state (V_{GS} > 0), energy bands in the channel region are pushed downward which leads to an overlap between the valence band of the source with the conduction band of the channel. This overlap opens a window for band-to-band tunneling of a large number of electrons in the valence band of the source to the conduction band of the channel. These electrons can flow from the channel to the drain through drift/diffusion mechanisms.

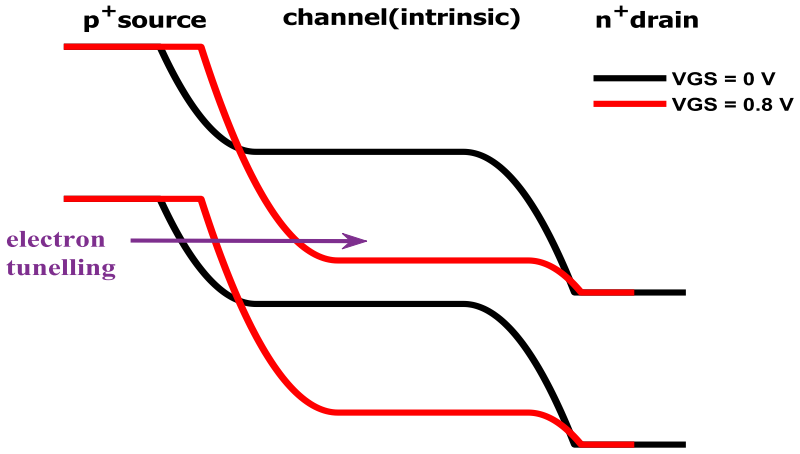

Fig. (1) the energy band diagram of TFET at OFF and ON state.

We now derive an expression for the distribution of electrical potential, that is the potential between the channel and the oxide of the gate, electric field, tunnelling generation rate, and then, the drain current for single-gate and double-gate TFET.

Assuming that the channel is intrinsic and neglecting free carriers, Poisson's equation. for the electric potential $\phi_{(x,y)}$ in the channel region can be written as (Laplace's equation) :

$$\frac{\partial^2 \emptyset_{(x,y)}}{\partial x^2} + \frac{\partial^2 \emptyset_{(x,y)}}{\partial y^2} = 0 \qquad (1)$$

The solution of this equation is assumed to be a parabolic approximation [18]:

$$\emptyset_{(x,y)} = C_{0(x)} + C_{1(x)} * y + C_{2(x)} * y^2 \qquad (2)$$

where the coefficients $C_{0(x)}$, $C_{1(x)}$ and $C_{2(x)}$ are functions of x only.

By applying the following boundary conditions:

$$\emptyset_{(x,0)} = \emptyset_{s(x)} \qquad (3)$$

$$\emptyset_{(0,y)} = V_{bi1} \qquad (4)$$

$$\emptyset_{(L_{ch},y)} = V_{bi2} + V_D \qquad (5)$$

$$\frac{\partial \emptyset_{(x,0)}}{\partial x} = \left(\frac{\epsilon_{ox}}{t_{ox}\epsilon_{si}}\right)\left(\emptyset_{s(x)} - V_{GS} + V_{FB}\right) \qquad (6)$$

$$\frac{\partial \emptyset_{(x,t_{si})}}{\partial x} = 0 \qquad (7)$$

For double-gate TFET Eq. (7) will be rewritten as.

$$\frac{\partial \emptyset_{(x,t_{si})}}{\partial x} = -\left(\frac{\epsilon_{ox}}{t_{ox}\epsilon_{si}}\right)\left(\emptyset_{s(x)} - V_{GS} + V_{FB}\right)$$

The meaning of all symbols is summarized in **Table 1**. Where V_{bi1} is built in potential at the source-channel junction $V_{bi1} = -V_{th} * \ln(\frac{N_s}{n_i})$, V_{th} is the thermal voltage, N_s is the doping concentration in the source, n_i is the intrinsic concentration , V_{bi2} is built in potential in the drain channel side$V_{bi2} = -V_{th} * \ln(\frac{N_D}{n_i})$, N_D is the doping concentration in the drain, V_{FB} is a flat band voltage $V_{FB} = \varphi_m - \chi - \frac{E_g}{2}$, φ_m is the metal work function, χ is the electron affinity, E_g the energy band gap, ϵ_{ox} is the relative permittivity of the oxide, ϵ_{si} is the relative permittivity of silicon and t_{ox} is the thickness of the oxide.

Table (1) Description of symbols

Symbol	Description	Unit
V_{bi1}	Built in potential at the source-channel side	V
V_{bi2}	Built in potential in the drain channel side	V
V_{th}	Thermal voltage that equals to 0.0259 in the room temperature	eV
N_s	Doping concentration in the source	cm^{-3}
N_D	Doping concentration in the drain	cm^{-3}
n_i	Intrinsic concentration	cm^{-3}
V_{FB}	Flat band voltage	eV
φ_m	Metal work function	eV
χ	Electron affinity	eV
E_g	Energy band gap	eV
ϵ_{ox}	Relative permittivity of the oxide	F/cm
ϵ_{si}	relative permittivity of silicon	F/cm
t_{ox}	Thickness of the oxide	nm
t_{si}	Thickness of the silicon substrate	nm

Then we can get the coefficients $C_{0(x)}$, $C_{1(x)}$, and $C_{2(x)}$ as a function of surface potential $\emptyset_{s(x)}$.

$$C_{0(x)} = \emptyset_{s(x)} \quad (8)$$

$$C_{1(x)} = \left(\frac{\epsilon_{ox}}{t_{ox}\epsilon_{si}}\right)\left(\emptyset_{s(x)} - V_{GS} + V_{FB}\right) \quad (9)$$

$$C_{2(x)} = \left(\frac{-\epsilon_{ox}}{2t_{ox}t_{si}\epsilon_{si}}\right)\left(\emptyset_{s(x)} - V_{GS} + V_{FB}\right) \quad (10)$$

For double-gate TFET Eq. (10) will be rewritten as.

$$C_{2(x)} = \left(\frac{-\epsilon_{ox}}{t_{ox}t_{si}\epsilon_{si}}\right)\left(\emptyset_{s(x)} - V_{GS} + V_{FB}\right)$$

Substituting Eqs. (8), (9), and (10) into Eq. (2), we obtain the following second-order differential equation:

$$\emptyset''_{s(x)} - K^2\,\emptyset_{s(x)} = K^2\,\emptyset_d \quad (11)$$

where $\emptyset_d = V_{FB} - V_{GS}$, for single-gate $K = \sqrt{\frac{\epsilon_{ox}}{t_{ox}t_{si}\epsilon_{si}}}$, for double-gate $K = \sqrt{\frac{2\epsilon_{ox}}{t_{ox}t_{si}\epsilon_{si}}}$

By solving Eq. (11) the surface potential is:

$$\emptyset_{s(x)} = Ae^{Kx} + Be^{-Kx} - \emptyset_d \quad (12)$$

Where A and B are expressed as,

$$A = \frac{-V_{bi1}e^{-Kl_{ch}} + \emptyset_d\left(1 - e^{-Kl_{ch}}\right) + V_{bi2} + V_{Ds}}{2\sinh(Kl_{ch})} \quad (13)$$

$$B = \frac{-V_{bi1}e^{Kl_{ch}} + \emptyset_d\left(1 - e^{Kl_{ch}}\right) + V_{bi2} + V_{Ds}}{-2\sinh(Kl_{ch})} \quad (14)$$

The potential is analytically derived as follows to determine the vertical and lateral electric fields (E_y) and (E_x) respectively.

$$E_y(x,y) = -\frac{\partial \emptyset_{(x,y)}}{\partial y} = -C_{1(x)} + 2yC_{2(x)} \quad (15)$$

$$E_x(x,y) = -\frac{\partial \emptyset_{(x,y)}}{\partial x} = -AKe^{Kx} + BKe^{-Kx} \quad (16)$$

Drain current is calculated by integrating the band-to-band generation rate (G) across volume of the tunnelling region.

$$I_D = q \int G_{BBT}\, dv \quad (17)$$

Where G_{BBT} is band to band generation rate

$$G_{BBT}(E) = AE^2 \exp\left(\frac{-B}{E}\right) \quad (18)$$

3. Modeling of ISFET:

The construction of the ISFET is the same as the conventional FET with the gate metal is replaced by an electrolyte with reference electrode as shown in **Figure. 2**. In this section, we will explain the mechanism that relates the pH value in an electrolyte solution of an ISFET with the electrostatics of the underling FET device. Specifically, it is aimed to relate the pH-value of the electrolyte with the potential on the insulator/electrolyte interface (ψ_0).

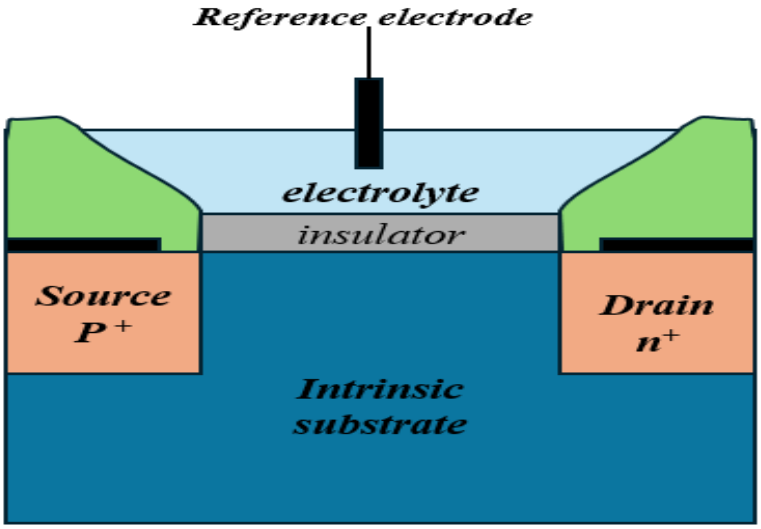

Fig. (2) construction of ISFET

A surface charge on the insulator is formed due to the release (deprotonation) or absorption (protonation) of a nearby proton H^+ of hydroxyl surface group. As shown in the following equations:

Deprotonation:

$$A - OH \leftrightarrow A - O^- + H_s^+ \text{ with } K_b = \frac{[A-O^-][H_s^+]}{[A-OH]} \quad (19)$$

Protonation:

$$A - OH_s^+ \leftrightarrow A - OH + H_s^+ \text{ with } K_a = \frac{[A-OH][H_s^+]}{[A-OH_s^+]} \quad (20)$$

where A is a symbol refers to any type of oxide, K_b and K_a are the base and acid dissociation constants respectively, $[H_s^+]$ is the proton concentration at the surface insulator, that is related to the bulk concentration $[H_b^+]$ as described in [19].

$$[H_s^+] = [H_b^+] \exp\left(\frac{q(V_{ref} - \psi_0)}{KT}\right) \quad (21)$$

where V_{ref} is the voltage of the reference electrode, q is the electronic charge, K is the Boltzmann constant, and T is the temperature. There are two other equations that determine the concentration of the surface species, the first equation is related to the amount of site binding charge per unit area.

$$N_s = [A - OH] + [A - O^-] + [A - OH_s^+] \quad (22)$$

and the second equation is related to surface charge per unit area

$$\sigma_0 = q([A - OH_s^+] - [A - O^-]) \quad (23)$$

Equations from (19) to (23) can be solved to get the relation between surface potential, σ_0, and pH.

$$[H_s^+] = \sqrt{K_a K_b}\exp\left(\frac{q\psi_0 - V_{ref}}{KT}\right) * \left[\frac{\left(\frac{\sigma_0}{qN_s\delta}\right) + \left[\left(\frac{\sigma_0}{qN_s\delta}\right)^2 + 1 + \left(\frac{\sigma_0}{qN_s}\right)^2\right]^{0.5}}{\left(1 - \frac{\sigma_0}{qN_s}\right)}\right] \quad (24)$$

By taking ln for Eq. (24) we can get [20]:

$$-2.303(pH - pH_{pzc}) = \left(\frac{q\psi_0 - V_{ref}}{KT}\right) + \sinh^{-1}\left(\frac{\sigma_0}{qN_s\delta}\right) - \ln\left(1 - \frac{\sigma_0}{qN_s}\right) \quad (25)$$

after some approximation we get the relation between pH and ψ_0 [19 – 21].

$$\psi_0 = -2.303 * (pH - pH_{pzc}) * V_{th} * \left(\frac{\beta}{1+\beta}\right) + V_{ref} \quad (26)$$

where pH is the concentration of Hydrogen ions of the electrolyte, pH_{pzc} (point of zero charge) is the value of pH at which the total charge on the surface equal zero (equal positive and negative charges), V_{th} is the thermal potential, and β is a constant that is given below.

$$pH_{pzc} = -\log\left(\sqrt{K_a K_b}\right) \quad (27)$$

$$V_{th} = \frac{KT}{q} \quad (28)$$

$$\beta = \frac{qN_s\delta}{V_t C_{eq}} \quad (29)$$

$$\delta = 2\sqrt{\frac{K_b}{K_a}} \quad (30)$$

$$C_{eq} = \frac{C_{st}C_{dl}}{C_{st} + C_{dl}} \quad (31)$$

$$C_{dl} = \sqrt{\frac{2qn_0\varepsilon_w Z_i^2}{V_t}} \quad (32)$$

where C_{st} is stern capacitance that has a constant value of $20*10^{-6}$ F/cm^2, C_{dl} is the double layer capacitance that is given by Eq. (32), n_0 is the ion concentration of the electrolyte, ε_w is the dielectric constant of the water, and Zi indicates the number of ith free ions in the valence shell. Here, we use NaCl in the electrolyte so Zi equal 1 as both Na^+ and Cl^- have valency of 1.

4. Proposed simulation method:

We discussed in section 2 the modelling of TFET and calculated the surface potential at a certain V_D and V_G see Eq. (12). We combined this equation with the equation of the surface potential of ISFET that we discussed in section 2 to solve the ISTFET **Figure. 3** shows the construction of ISTFET. Many previous works use the approximate Eq. (26) to relate the surface potential with the pH value, in which σ_0 is neglected. The idea of our work is to use the more accurate form given in Eq. (25) and use iterative method to solve for the surface potential ψ_0. The methodology is shown in the flow chart in **Figure 4**.

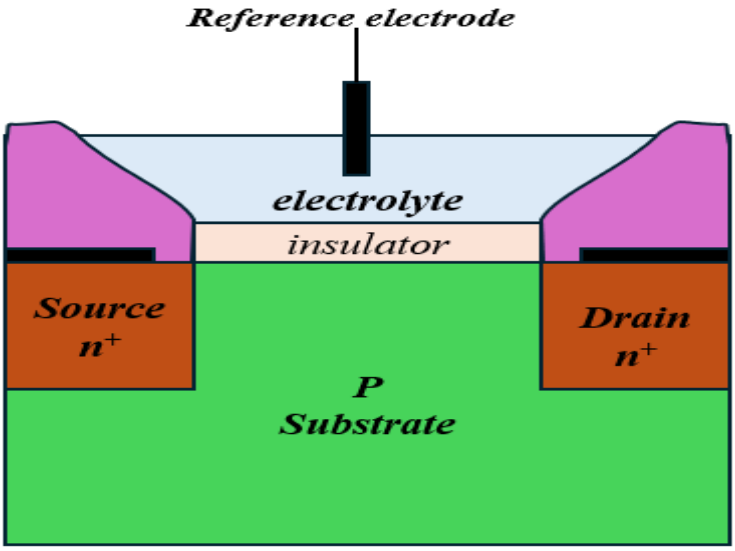

Fig. (3) construction of ISTFET

$$\psi_0 = \left[-2.303 * (pH - pH_{pzc}) - \sinh^{-1}\left(\frac{\sigma_0}{qN_s\delta}\right)\right] * V_t + V_{ref} \quad (33)$$

$$\sigma_0 = qN_s\left(\frac{[H_s^+]^2 - K_aK_b}{[H_s^+]^2 + [H_s^+]K_a + K_aK_b}\right) \quad (34)$$

We rewrite Eq. (12) using Eq. (34)

$\emptyset_{s(x)} = Ae^{Kx} + Be^{-Kx} - \emptyset_d$, Where $\emptyset_d = V_{FB} - \psi_0$

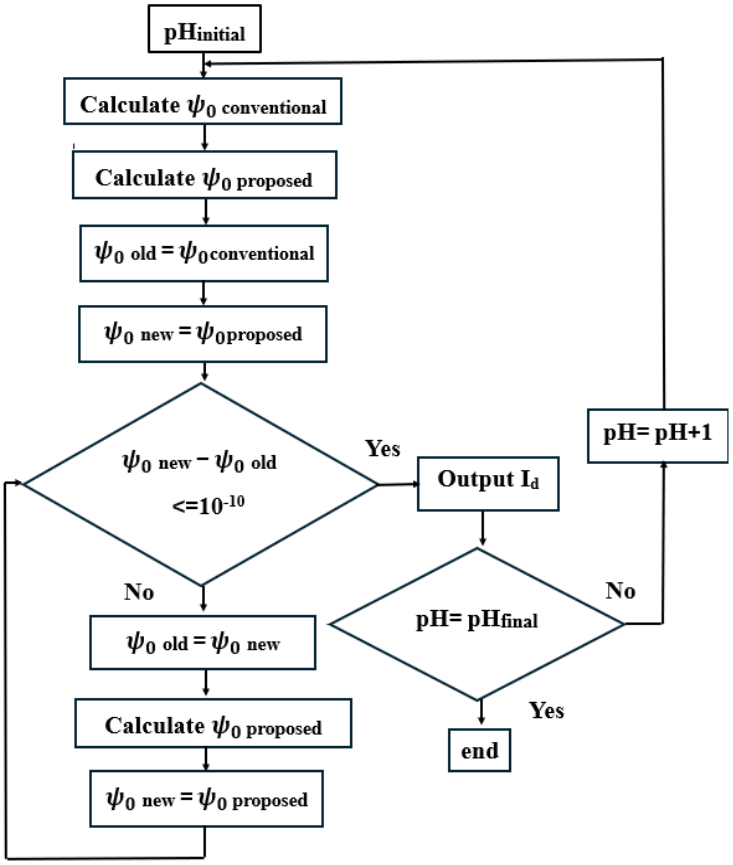

Fig. (4) Flow chart for the methodology proposed for the extraction of ISTFET sensitivity.

Regarding the current calculation, it is usually calculated using an average tunneling path length [24]. We propose here a methodology for calculating a non-local tunneling generation rate resulted from a variable tunneling path as explained hereinafter. We define the starting point of tunnelling as the point at which the surface potential increases by Eg/q where Eg is the energy gap. On the other hand, the end point is determined by the edge of the conduction band of the drain as shown in **figure (5.a),** and **(5.b).**

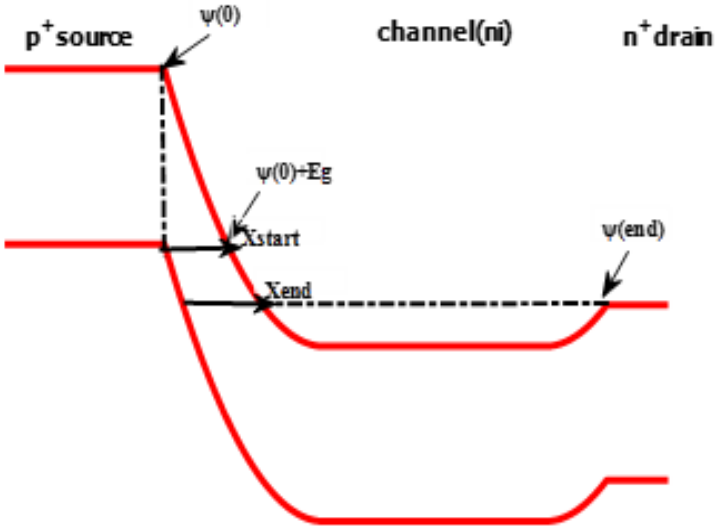

(a)

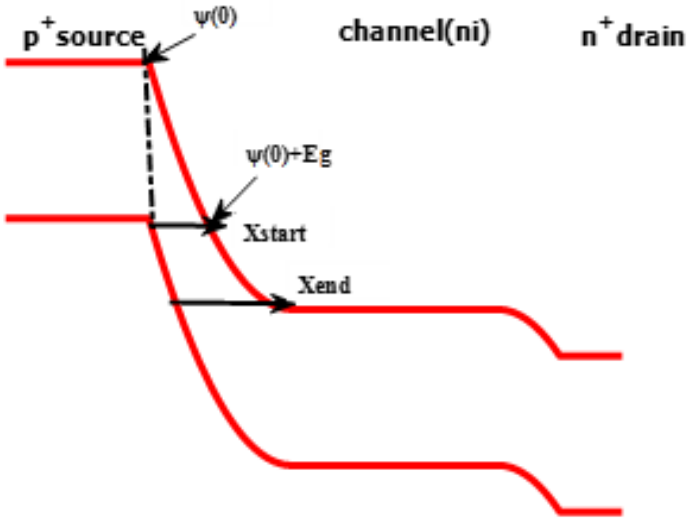

(b)

Fig. (5) (a), and(b) show the energy band diagram of TFET in two cases of gate and drain voltage to get the length of the tunnelling(a)the edge of the conduction band of the drain is higher than the edge of conduction band of the channel (b) the conduction band of the drain lower than the conduction band of the channel.

Between the starting and end points, we can calculate the generation rate at each point by calculating the average electric field that produces tunnelling at that point. This is implemented as follows: we first calculate the average electric field within a potential energy change equal to Eg behind the point of consideration, then we use this average electric field to calculate the generation rate at this point. This is repeated for all points from the start to the end points. The drain current is then calculated by integrating the generation rates over the relevant range.

We can then calculate the sensitivity of the ISFET for pH change. There are two methods of measuring ISFET sensitivity: (1) current sensitivity (S_1) and voltage sensitivity (S_2). S_1 is defined as the change of drain current per unit change in pH with fixed reference voltage V_{ref}. On the other hand, S_2 is defined as the change in reference voltage that is required to maintain the drain current I_d unchanged when pH is changed by one unit. S_1 and S_2 can be expressed mathematically as follows:

$$S_1 = \left|\frac{\partial I_d}{\partial pH}\right|_{fixed\ V_{ref}} \quad (35)$$

$$S_2 = \left|\frac{\partial V_{ref}}{\partial pH}\right|_{fixed\ I_D} \quad (36)$$

5. Results and discussions

The values of various parameters used in the simulation are shown in **Tables 2** and **3**. The drain voltage (V_D) is set to 0.5V for all simulations, and for simplicity the device width is taken to be 1 μm and the channel is assumed to be intrinsic. First, our model is validated by comparing the drain current calculated from the model to the Silvaco TCAD simulation. **Figure .6** shows the drain current versus gate voltage for our model and for TCAD simulation. **Table 4** shows the key device metrics, such as I_{OFF}, I_{ON}, and subthreshold swing (SS) for our model and TCAD. For reference voltages above 0.7 V, the model results agree with simulation results with maximum error up to 5.1%. For very small reference voltages (below 0.5 V), drain current levels are so small that become comparable to roundoff errors of computations used in TCAD tool. In **Figure. 7(a)** and **(b)** we illustrate the vertical and latural electric field respectivily.

Table 2 general parameters

ϵ_w	80	W_{ch}	1 μm
c_0	10^{13} cm^{-3}	q	1.6×10^{-19} C
c_{st}	20×10^{-6} F/cm^2	K_B	1.38×10^{-23} J/K
φ_m	4.5 eV	n_i	10^{10} cm^{-3}
χ	4.05 eV	N_D	5×10^{18} cm^{-3}
V_D	0.5 V	N_s	10^{20} cm^{-3}
L_{ch}	30×10^{-7} cm	N_C	10^{10} cm^{-3}

Tabel 3 Values of site bending parameters of SiO_2, Al_2O_3, and HfO_2.

Dielectric	Relative permittivity (ϵ_r)	Dissociation constant (K_a)	Dissociation constant (K_b)	N_s (cm^{-2})
SiO_2	3.7	10^{2}	10^{-6}	5×10^{14}
Al_2O_3	9	10^{-6}	10^{-10}	8×10^{14}
HfO_2	25	10^{-7}	10^{-7}	4×10^{14}

Table 4 the key device metrics

	I_{OFF}	I_{ON}	(SS)
TCAD	6.6×10^{-17} A	1.28×10^{-7} A	20 mV/decade
Our Model	8.9×10^{-17} A	1.08×10^{-7} A	25 mV/decade

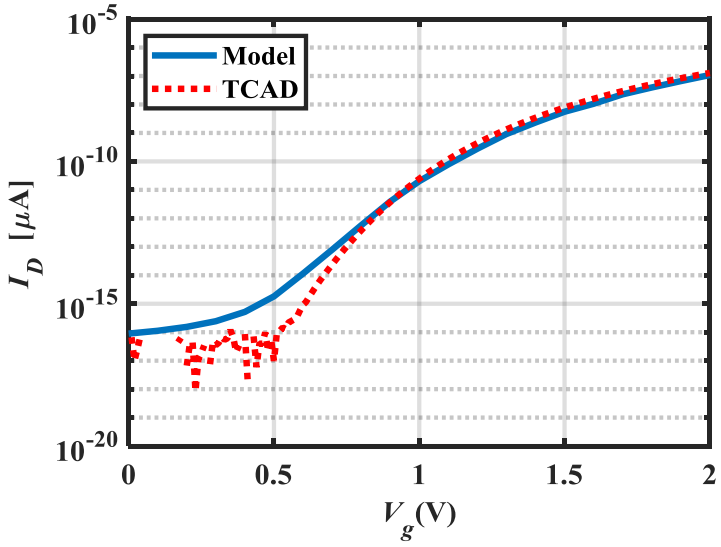

Fig. (6) Drain current Vs gate voltage by the model and TCAD simulation

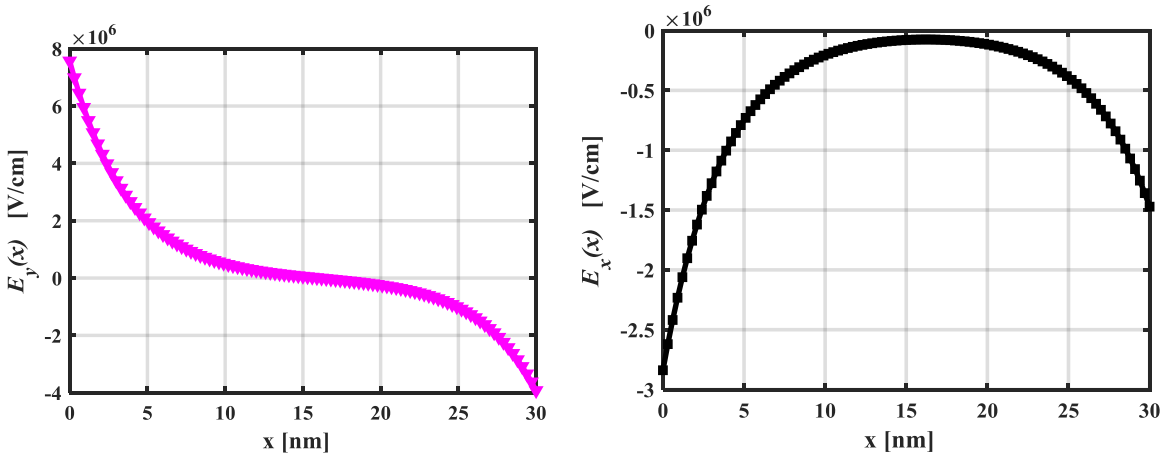

Fig.7(a) vertical electric field (b) latural electric field.

In **Figue. 8** the drain current is plotted versus the reference voltage for both (a) single-gate and (b) double-gate configurations. A SiO_2 insulator of thickness 3 nm is used, and results are extracted for three different pH values (pH = 4, 7, and 10). It is found from the result that the ratio of the currents in the double gate to the single gate is nearly equal to 10. It is clear that, for high pH, the current decreases due to the decrease of $[H_b^+]$ ($[H_b^+] = 10^{-pH}$), which leads to the decrease of charge on the surface and so does the drain current. In double gate the current is higher than in the single gate TFET that is due to increase of the tunnelling area it will result in increase the sensitivity. This is explained from the energy band-diagram given in **Figure. 9** where decreasing pH value leads to lowering energy bands, which decreases the tunneling length and so the current increases. For the rest of figures we get results for single gate. Results for double gate will be similar with just higher levels of current.

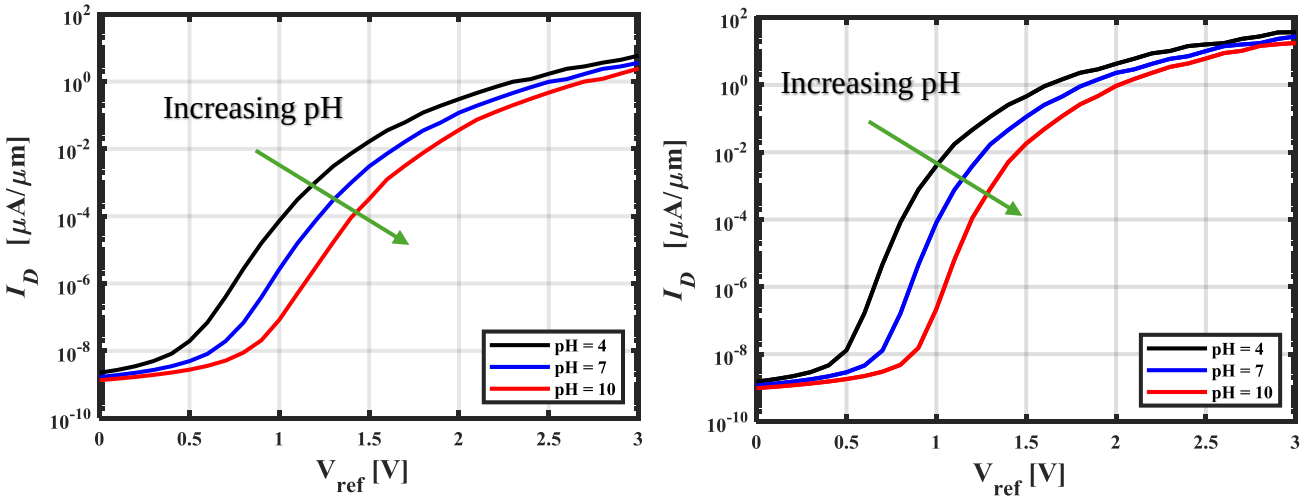

(a) (b)

Fig. (8) Drain current Vs Vref for pH =4,7, and10 (a)for single gate (b) for double gate.

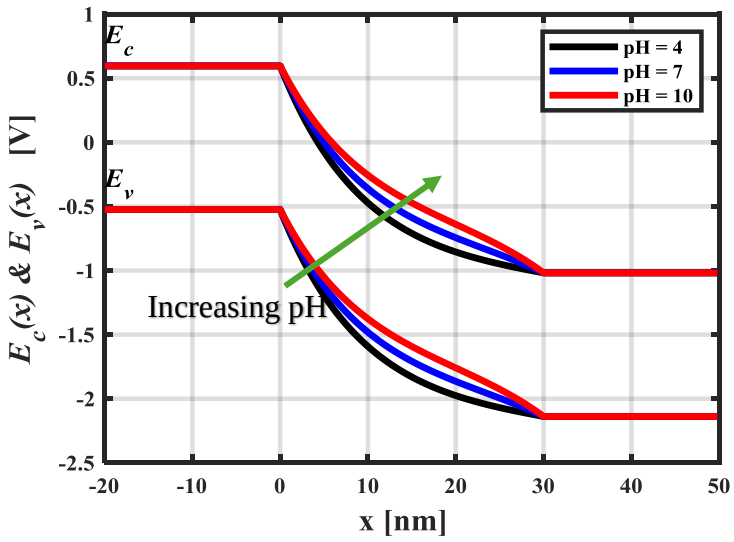

Fig. (9) energy band diagram for pH = 4, 7, and 10

The impact of various ISFET pH sensor parameters on the output current and the sensor sensitivities S_1 and S_2 is next investigated using the proposed simulation tool.

Regarding the current sensitivity S_1, we first plot the change of the current versus the pH value for different values of V_{ref} as depicted in **figure. 10**. As shown in fig. (10), for low V_{ref} (V_{ref} = 0.3 and 0.6 V), the change in current is not perceptible in the high pH range and, moreover, the linearity is very poor. Consequently, it is recommended to choose V_{ref} higher than 0.9 V. Further illustrated in **Figure. 11** where S_1 is plotted versus pH for V_{ref} = 0.9, 1.2, 1.5, and 1.8 V. From the figure it's clear that for low V_{ref} the sensitivity is relatively smaller. The sensitivity for V_{ref} = 0.9 V is about two orders of magnitude less than

that at V_{ref} = 1.8 V. In addition, for low $V_{ref,}$ S_1 varies more noticeably over the pH range which means less stability and linearity.

The average sensitivity is the mean of the sensitivity over all the pH values from 1 to 14. The average sensitivity is affected by many parameters such as oxide thickness, substrate thickness, type of the oxide, and the temperature. In **Figure. 12** $S_{1,\,av}$ is plotted versus V_{ref} for SiO_2 insulator of thickness t_{ox} = 3, 5, and 7 nm . It is noted that $S_{1,\,av}$ decreases when increasing t_{ox}. This is because of the reduction of the coupling between the carrier transport in the channel and the floating gate voltage. On the other hand, **Figure. 13** shows the effect of the substrate thickness t_{si} which is taken to be = 10, 15, and 20 nm. Here, $S_{1,\,av}$ also decreases with increasing t_{si} because the drain current decreases as the substrate thickness rises because the gate-channel coupling deteriorates. **Figure. 14** shows the effect of the type of the oxide where three types of the oxides SiO_2, Al_2O_3, and HfO_2 are used all with t_{ox} = 3nm and t_{si} = 10 nm. The more the dielectric constant of the oxide, the more is the sensitivity. Higher dielectric constant means higher gate control and larger drain current.

Turning to the effect of the temperature, **Figure. 15** shows the change of ISTFET average sensitivity ($S_{1,\,av}$) with temperature for a temperature range 260 – 340 K. it's clear from the figure that the average sensitivity increases with increasing the temperature that is due to increasing the number of tunnelling electrons.

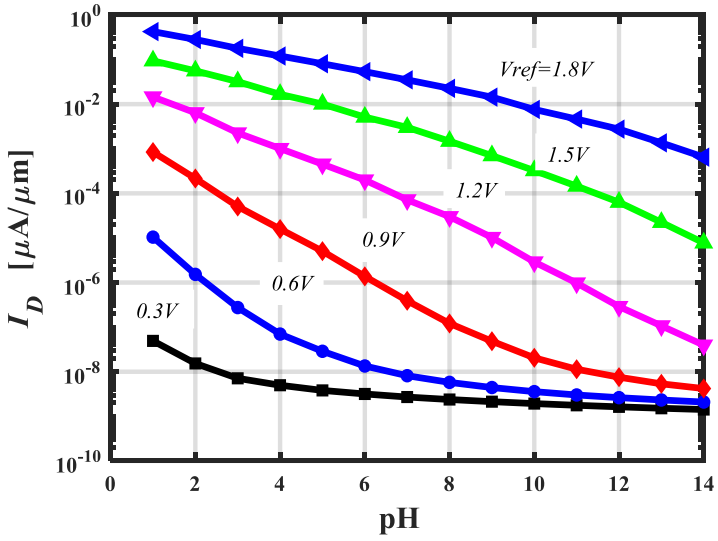

Fig. (10) change of drain current Vs pH for Vref = 0.3, 0.6, 0.9, 1.2, 1.5, 1.8V for SiO_2 insulator and t_{si} = 3nm

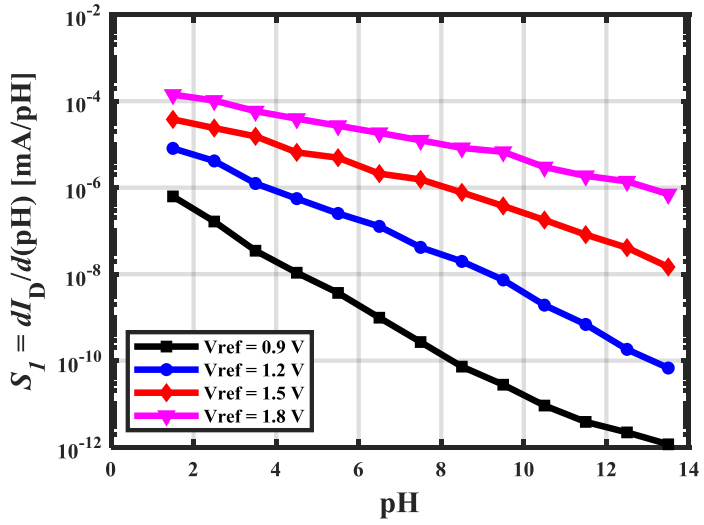

Fig. (11) The sensitivity S_1 along the pH range for SiO_2 insulator of t_{ox} = 3 nm at four values of

Vref = 0.9, 1.2, 1.5, and 1.8 V.

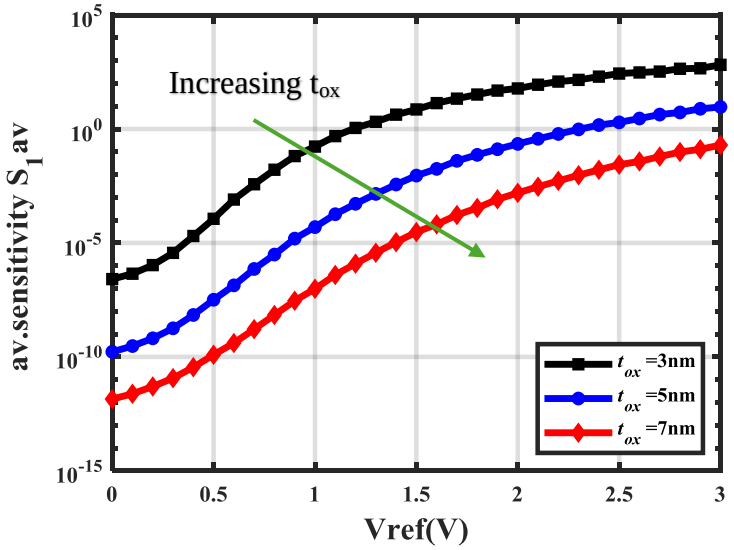

Fig. (12) The average sensitivity $S_{1,av}$ along the pH range is plotted Vs V_{ref} for SiO_2 insulator of three different thickness t_{ox} = 3, 5, and 7 nm.

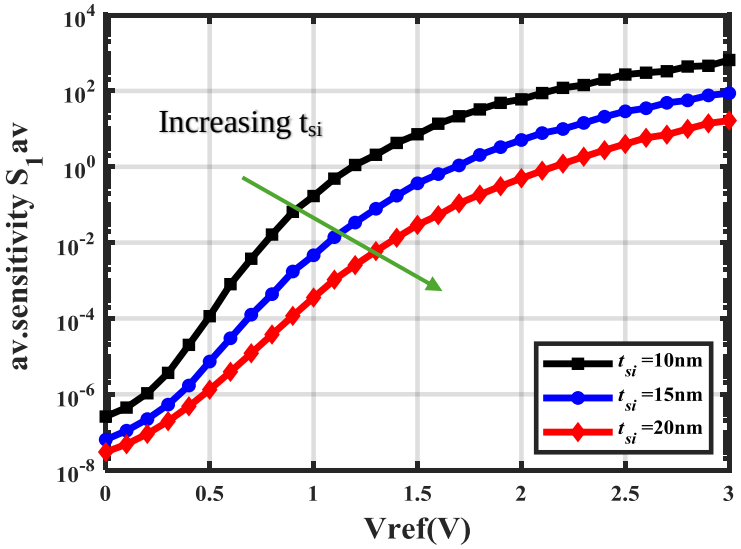

Fig. (13) The average sensitivity $S_{1,av}$ along the pH range is plotted Vs Vref for SiO_2 insulator of three different thickness of the substrate t_{si} = 10, 15, and 20 nm.

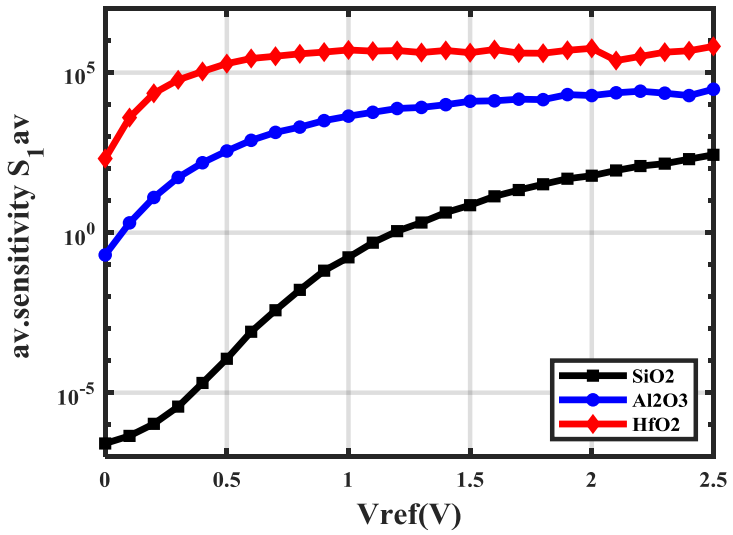

Fig. (14) The average sensitivity $S_{1,av}$ along pH range is plotted Vs V_{ref} for three different insulator types: SiO_2, Al_2O_3, and HfO_2 for t_{ox} = 3 nm.

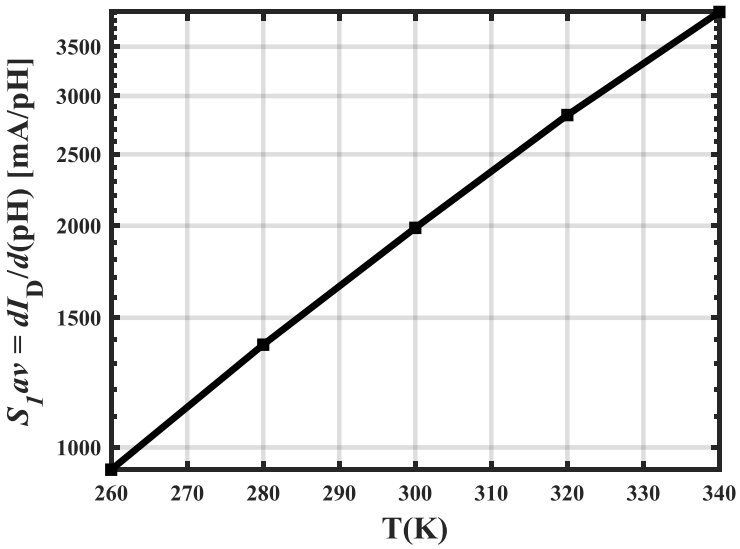

Fig. (15) The average sensitivity $S_{1,av}$ along pH range is plotted Vs V_{ref} for five values of temperature = 260, 280, 300, 320, and 340 K for AL_2O_3 insulator for t_{ox} = 3 nm and V_{ref} =0.8V.

Another type of sensitivity, S_2, is defined as the change in V_{ref} required to maintain the drain current at a predefined value. We compare here the proposed simulation method explained in section 4 with the conventional approximated method used elsewhere. **Figure. (16.a)** and **(16.b)** show the average sensitivity $S_{2,av}$ across the whole pH range versus the drain current for two different types of insulators: Al_2O_3, and HfO_2 ,respectively for both conventional approximated and new proposed simulation methods.

In **Figure. 17** we draw the diffrence between the proposed and conventional surface potential against the reference voltage. Although the diffrence between the two methods is small it is about 2.1 mV, but its effect is very clear in the sensiyivity. The error in the average sensitivity $S_{2,av}$ is reach 2.3%.

Regarding the effects of oxide thickness, substrate thickness, and temperature on the average sensitivity $S_{2,av}$ it is evident from **Figure. 18** and **19** that $S_{2,av}$ is insensitive to changes in either oxide thickness or substrate thickness and it is preserved at around 60

mV/pH. **Figure. 20** shows $S_{2,av}$ plotted against temperature. As the temperature increases, the average sensitivity also increases.

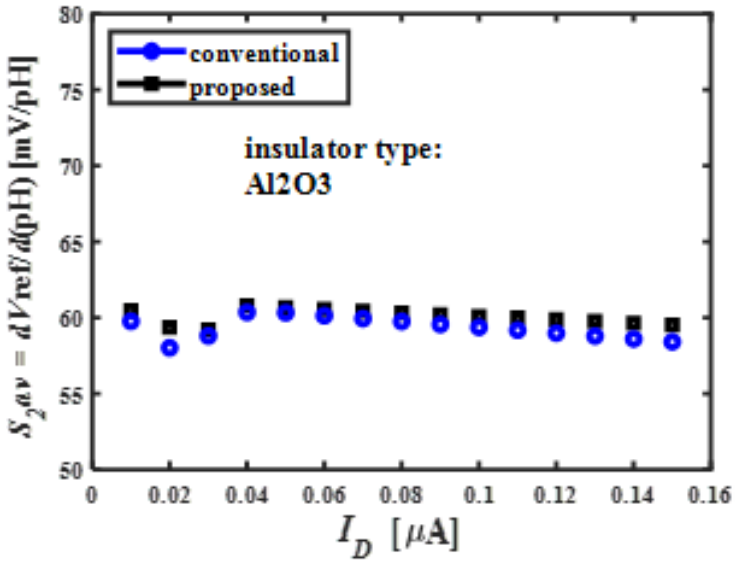

(a)

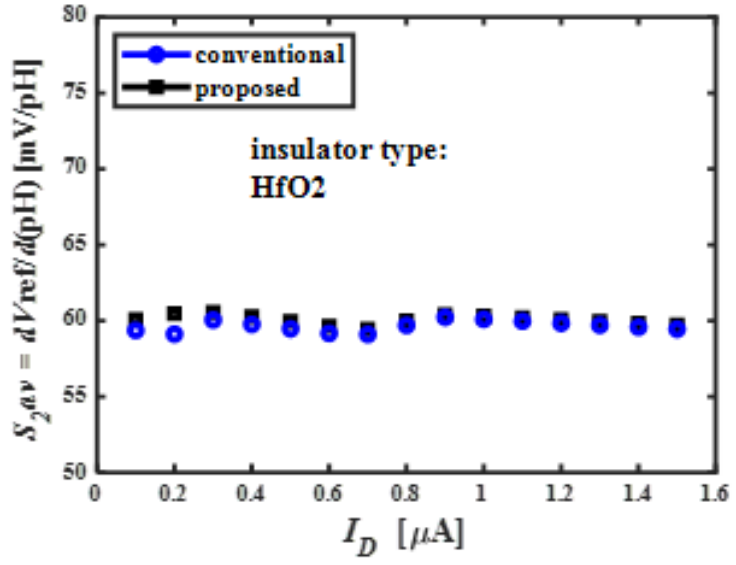

(b)

Fig. (16) (a), and (b) shows the average sensitivity $S_{2,av}$ along the pH range versus various drain current for conventional and proposed method of the surface potential (a)$S_{2,av}$ Vs I_d for Al_2O_3 (b) $S_{2,av}$ Vs I_d for HfO_2 .

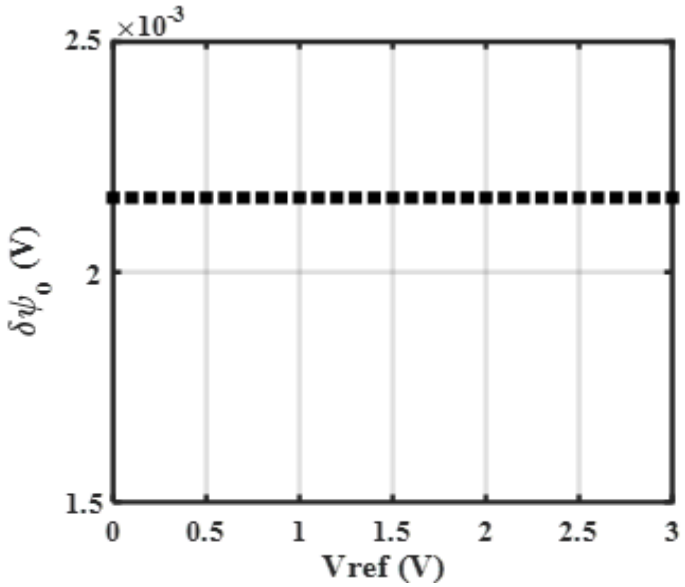

Fig. (17) the difference between the proposed and conventional surface potential versus the reference voltage.

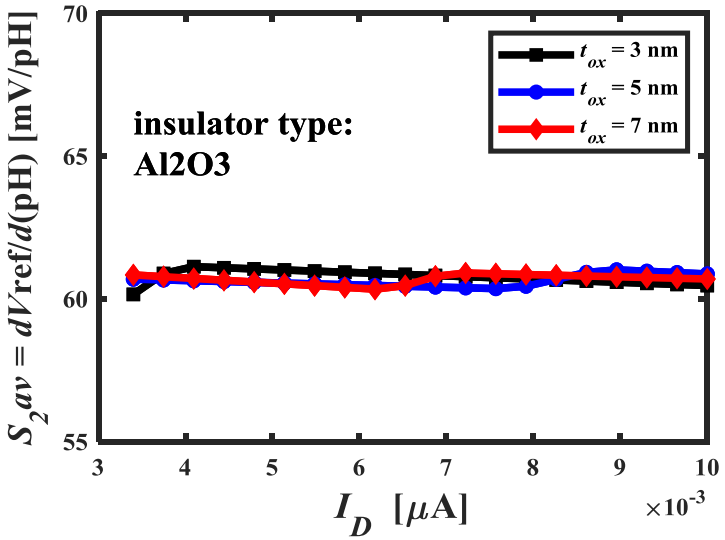

Fig. (18) The average sensitivity $S_{2,\,av}$ along the pH range is plotted Vs I_d for Al_2O_3 insulator of three different thickness t_{ox} = 3, 5, and 7 nm.

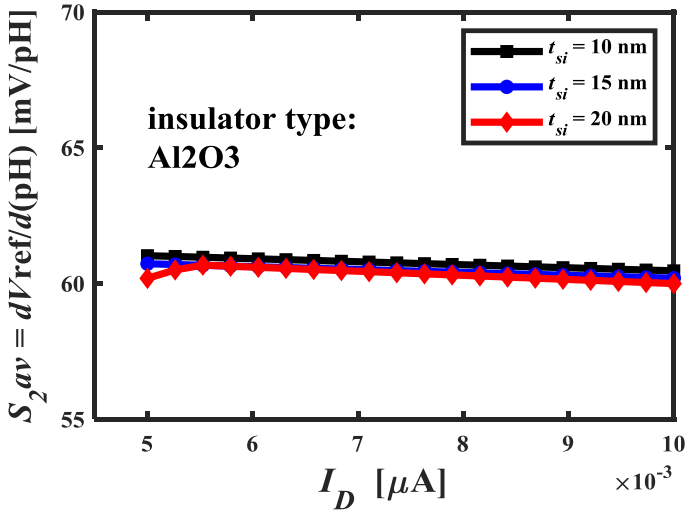

Fig. (19) The average sensitivity $S_{2,av}$ along the pH range is plotted Vs I_d for Al_2O_3 insulator of three different thickness of the substrate t_{si} = 10, 15, and 20 nm

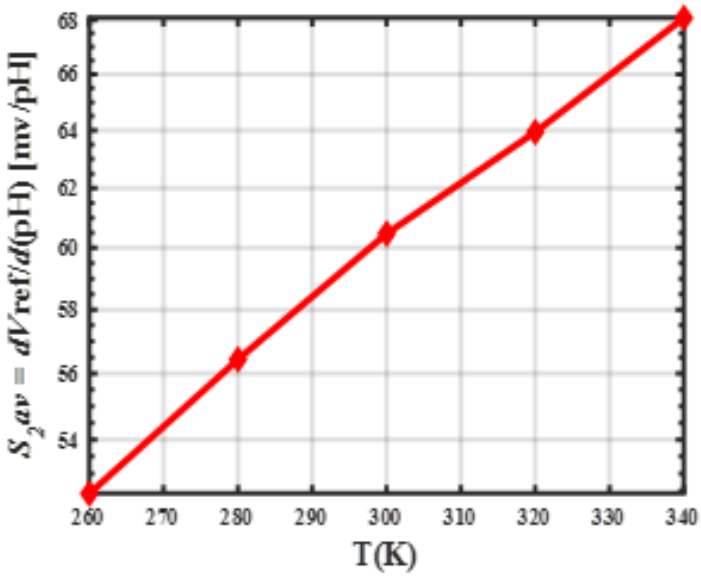

Fig. (20) The average sensitivity $S_{2,av}$ along the pH range is plotted Vs temperature for Al_2O_3 of t_{ox} = 3 nm and I_d = 0.2µA.

6. Conclusion:

A numerical simulation tool has been developed for nanoscale Ion-Sensitive Tunnelling Field-Effect-Transistor (ISTFET). The tool combines Gouy-Chapman-Stern equations with TFET modelling equations to find output device current and to calculate current and voltage sensitivities. The tool uses a novel iterative method to find the potential on the insulator/ electrolyte interface at certain pH value. It gives more accurate results than that found using conventional method used in the literature we can get more accurate results as we don't neglect any parameter, and it also improved the values of the sensitivity. The difference between the two methods in calculating the potential is about 2.1 mV. The diffference is smal but has clear effect on the sensitivity.The tool is used to find the optimum settings that lead to the highest sensitivity and linearity of pH measurement. It was found that S_1 varies significantly over the pH range, indicating nonlinear measurement. Furthermore, it is demonstrated that S_1 increases with temperature and decreases with increasing gate-insulator and substrate thickness. Conversely, S_2 is found to be invariant for a wide range of current levels and across the whole pH range. Furthermore, neither the substrate thickness nor the gate-insulator thickness has an impact on S_2 it is around 60 mV/pH. Three different insulator types

SiO_2, Al_2O_3, and HfO_2 are compared and it was concluded that the sensitivity of Al_2O_3 and HfO_2 are significantly higher than that of SiO_2.

References

[1] P. Bergveld, "The development and application of FET-based biosensors," Biosensors (Basel), vol. 2, no. 1, pp. 15–33, Jan. 1986, doi: 10.1016/0265-928X(86)85010-6.

[2] X. Chen et al., "Electrical nanogap devices for biosensing," Materials Today, vol. 13, no. 11, pp. 28–41, Nov. 2010, doi: 10.1016/S1369-7021(10)70201-7.

[3] R. E. G. van Hal, J. C. T. Eijkel, and P. Bergveld, "A novel description of ISFET sensitivity with the buffer capacity and double-layer capacitance as key parameters," Sens Actuators B Chem, vol. 24, no. 1–3, pp. 201–205, Mar. 1995, doi: 10.1016/0925-4005(95)85043-0.

[4] D. E. Yates, S. Levine, and T. W. Healy, "Site-binding model of the electrical double layer at the oxide/water interface," Journal of the Chemical Society, Faraday Transactions 1: Physical Chemistry in Condensed Phases, vol. 70, no. 0, pp. 1807–1818, Jan. 1974, doi: 10.1039/F19747001807.

[5] T. M. Abdolkader, "A numerical simulation tool for nanoscale ion-sensitive field-effect transistor," International Journal of Numerical Modelling: Electronic Networks, Devices and Fields, vol. 29, no. 6, pp. 1118–1128, Nov. 2016, doi: 10.1002/jnm.2170.

[6] J. Go, P. R. Nair, B. Reddy, B. Dorvel, R. Bashir, and M. A. Alam, "Coupled heterogeneous nanowire-nanoplate planar transistor sensors for giant (>10 V/pH) nernst response," ACS Nano, vol. 6, no. 7, pp. 5972–5979, Jul. 2012, doi: 10.1021/NN300874W/SUPPL_FILE/NN300874W_SI_001.PDF.

[7] P. Dwivedi, R. Singh, and Y. S. Chauhan, "Crossing the Nernst Limit (59 mV/pH) of Sensitivity through Tunneling Transistor-Based Biosensor," IEEE Sens J, vol. 21, no. 3, pp. 3233–3240, Feb. 2021, doi: 10.1109/JSEN.2020.3025975.

[8] C. H. Chu et al., "Beyond the Debye length in high ionic strength solution: direct protein detection with field-effect transistors (FETs) in human serum," Scientific Reports 2017 7:1, vol. 7, no. 1, pp. 1–15, Jul. 2017, doi: 10.1038/s41598-017-05426-6.

[9] N. Kumar, J. Kumar, and S. Panda, "Enhanced pH sensitivity over the Nernst limit of electrolyte gated a-IGZO thin film transistor using branched polyethylenimine," RSC Adv, vol. 6, no. 13, pp. 10810–10815, Jan. 2016, doi: 10.1039/C5RA26409J.

[10] N. Liu, Y. Hui Liu, P. Feng, L. Qiang Zhu, Y. Shi, and Q. Wan, "Enhancing the pH sensitivity by laterally synergic modulation in dual-gate electric-double-layer transistors," Appl Phys Lett, vol. 106, no. 7, Feb. 2015, doi: 10.1063/1.4913445/28555.

[11] J. Go, P. R. Nair, B. Reddy, B. Dorvel, R. Bashir, and M. A. Alam, "Beating the Nernst limit of 59mV/pH with double-gated nano-scale field-effect transistors and its applications to ultra-sensitive DNA biosensors," Technical Digest - International Electron Devices Meeting, IEDM, 2010, doi: 10.1109/IEDM.2010.5703325.

[12] D. Il Moon, J. W. Han, and M. Meyyappan, "Comparative Study of Field Effect Transistor Based Biosensors," IEEE Trans Nanotechnol, vol. 15, no. 6, pp. 956–961, Nov. 2016, doi: 10.1109/TNANO.2016.2615855.

[13] P. Singh, D. P. Samajdar, and D. S. Yadav, "Doping and Dopingless Tunnel Field Effect Transistor," in 2021 6th International Conference for Convergence in Technology, I2CT 2021, Institute of Electrical and Electronics Engineers Inc., Apr. 2021. doi: 10.1109/I2CT51068.2021.9418076.

[14] P. Bal, M. W. Akram, P. Mondal, and B. Ghosh, "Performance estimation of sub-30 nm junctionless tunnel FET (JLTFET)," J Comput Electron, vol. 12, no. 4, pp. 782–789, Dec. 2013, doi: 10.1007/S10825-013-0483-6/FIGURES/13.

[15] A. Bhattacharyya, D. De, and M. Chanda, "Temperature Imposed Sensitivity Issues of Hetero-TFET Based pH Sensor," IEEE Trans Nanobioscience, vol. 22, no. 2, pp. 438–446, Apr. 2023, doi: 10.1109/TNB.2022.3202242.

[16] R. S. C. Cobbold, "Basic Properties of the Electrolyte-SiO2-Si System: Physical and Theoretical Aspects," IEEE Trans Electron Devices, vol. 26, no. 11, pp. 1805–1815, 1979, doi: 10.1109/T-ED.1979.19690.

[17] T. S. Arun Samuel, N. B. Balamurugan, S. Bhuvaneswari, D. Sharmila, and K. Padmapriya, "Analytical modelling and simulation of single-gate SOI TFET for low-power applications," International Journal of Electronics, vol. 101, no. 6, pp. 779–788, Jun. 2014, doi: 10.1080/00207217.2013.796544.

[18] Y. Yahia, M. S. Salem, A. Shaker, H. Kamel, M. Abouelatta, and M. ElBanna, "A modified pseudo

2D physically-based model for double-gate TFETs: Role of precise calculations of drain and source depletion regions," Ain Shams Engineering Journal, vol. 13, no. 1, Jan. 2022, doi: 10.1016/j.asej.2021.06.025.

[19] M. Grattarola, G. Massobrio, and S. Martinoia, "Modeling H+-Sensitive FET's with SPICE," 1992.

[20] "Operation of Chemically Sensitive Field-Effect Sensors As a Function of the Insulator-Electrolyte Interface."

[21] D. E. Yates, S. Levine, and T. W. Healy, "Site-binding Model of the Electrical Double Layer at the Oxide/ Wa t er Iiit er face Recent calculations 2 *," 1974.

[22] "Operation of Chemically Sensitive Field-Effect Sensors As a Function of the Insulator-Electrolyte Interface."

[23] D. Landheer, G. Aers, W. R. McKinnon, M. J. Deen, and J. C. Ranuarez, "Model for the field effect from layers of biological macromolecules on the gates of metal-oxide-semiconductor transistors," J Appl Phys, vol. 98, no. 4, Aug. 2005, doi: 10.1063/1.2008354.

[24] T. S. Arun Samuel and N. B. Balamurugan, "An analytical modeling and simulation of dual material double gate tunnel field effect transistor for low power applications," Journal of Electrical Engineering and Technology, vol. 9, no. 1, pp. 247–253, Jan. 2014, doi: 10.5370/JEET.2014.9.1.247.